Unpolarized emissivity of thin oil films over anisotropic Gaussian seas in infrared window regions

Nicolas Pinel,[1,*] Christophe Bourlier,[1] and Irina Sergievskaya[2]

[1]Université Nantes Angers Le Mans—IREENA Laboratory, Polytech'Nantes, Rue Christian Pauc, La Chantrerie, BP 50609, 44306 Nantes Cedex 3, France

[2]Institute of Applied Physics, Russian Academy of Sciences, Ul'yanova Street 46, Nizhny Novgorod 603600, Russia

*Corresponding author: nicolas.pinel@univ-nantes.fr

Received 9 November 2009; revised 23 February 2010; accepted 24 February 2010; posted 25 February 2010 (Doc. ID 119749); published 7 April 2010

In this paper, we derive the unpolarized infrared (IR) emissivity of thin oil films over anisotropic Gaussian seas from a refined physical surface spectrum model of damping due to oil. Since the electromagnetic wavelength is much smaller than the surface mean curvature radius and than the surface root mean square height, the Kirchhoff–tangent plane approximation, reduced to the geometric optics approximation, can be used. The surface can then be replaced by its local infinite tangent plane at each point of each rough surface. The multiple reflections at each interface are ignored (i.e., for both the upper air/oil interface and the lower oil/sea interface of the contaminated sea). Nevertheless, the multiple reflections between the upper and the lower interfaces of the oil film are taken into account, by assuming a locally flat and planar thin oil film, which forms a local Fabry–Perot interferometer. This means that the Fresnel reflection coefficient of a single interface can be substituted for the equivalent Fresnel reflection coefficient of the air/oil/sea film, calculated by considering an infinite number of reflections inside the layer. Comparisons of the emissivity between a clean sea and a contaminated sea are presented, with respect to emission angle, wind speed, wind direction, oil film thickness, oil type, and wavelength. Thus, oil detection, characterization, and quantization are investigated in the IR window regions.

OCIS codes: 290.5880, 000.5490, 010.4458, 260.3060, 280.4991, 240.0310.

1. Introduction

Remote sensing, by either radar or optical imagery, can be used to detect and monitor possible oil slicks on sea surfaces [1,2]. For optical applications, in order to act quickly when marine oil pollutions occur, it is then essential to dispose of a means that can predict the electromagnetic response from oil films on the sea, compared to the clean sea case. Here we will concentrate on emissivity, which quantifies the intrinsic radiation of the surface. Then, by calculating the contrast between a sea covered in oil (called a contaminated sea) and a clean sea, it is possible to evaluate the detectability of marine pollutions. Moreover, in order to have better direction of oil spill countermeasures, oil type characterization and quantization are of interest and are investigated here. If this is possible, it should make it possible to determine the origin of the oil spill, as well as the amount of oil that must be treated.

It has been established that for an accuracy of 0.3 K [which is a typical sensitivity of actual infrared (IR) sensors] on the sea surface temperature, the error in the emissivity must be less than approximately 0.5% [3]. Consequently, the sea surface emissivity must be determined with accuracy. For thermal IR applications, since the electromagnetic wavelength λ is much smaller than the sea surface mean curvature radius R_c, the tangent plane approximation (usually called the Kirchhoff approximation) can be applied. The surface can then be replaced by its local infinite tangent plane at each point of the surface. Moreover, because the electromagnetic wavelength

0003-6935/10/112116-16$15.00/0

λ is also much smaller than the surface root mean square (RMS) height σ_h, the geometric optics approximation (GOA) can be applied for sealike surfaces. Indeed, at IR frequencies, the capillary waves of sea surfaces also have a large mean curvature radius and a large RMS height compared to the wavelength λ.

As developed in [4,5], emissivity can be derived from the hemispherical reflectivity, for which the sea surface is assumed to be Gaussian and anisotropic. In [6], the shadowing effect is taken into account in order to improve the results, especially for low-grazing angles. The hemispherical reflectivity is obtained from integrating the reflectivity over the upper half space (above the sea surface). In this paper, this way is not used because the formulation is more complicated and because the surface reflectivity is necessary only for the calculation of the sun glint. Previous work, especially of Otremba and Piskozub [7–10], as well as of other authors, such as [11–14], deals with this topic at optical or IR bands, by considering flat surfaces. Besides, as done by de Beaucoudrey, Schott and Bourlier [15] from the GOA and by assuming 1D interfaces (i.e., for a 2D problem), the reflectivity of an oil film over a rough seawater can be computed from a Monte-Carlo method. This process requires generating a great number of incident photons, which interact with the rough interfaces generated from a spectral method and considering the Cox and Munk slope distribution [16].

In this paper, from an analytical approach based on the work of Bourlier [17], the unpolarized emissivity of thin oil films over 2D anisotropic rough sea surfaces (i.e., for a general 3D problem) is derived by using the GOA. We concentrate here on the case of homogeneous insoluble oil films, which restricts the validity domain of our study to low to moderate wind speeds at 10 m above the sea surface, that is to say u_{10} less than 8–10 m/s [18,19]. The clean and contaminated sea surfaces are assumed to be Gaussian. The influence of the non-Gaussianity of sea surfaces on the emissivity was studied by Bourlier for clean seas [17]. Then it was shown that the non-Gaussianity has only a slight influence on emissivity (much inferior to the influence of the multiple reflections at the same interface), and it is significant only for grazing observation angles θ and for moderate to high wind speeds u_{10}, and around upwind and downwind directions. Following the Cox and Munk experimental results [20,21] for contaminated seas, the skewness is unchanged, while the skewness is damped. This means that the emissivity contrast between clean and contaminated seas is slightly modified if non-Gaussian statistics is considered by the amount of skewness effect of clean seas, as described in [17], for grazing observation angles θ and for moderate to high wind speeds u_{10}, and around upwind and downwind directions. The multiple reflections at each interface are ignored (i.e., about the contaminated case, for both the upper air/oil interface and the lower oil/sea interface). For a clean sea surface, this phenomenon was studied by Henderson *et al.* [22] from a Monte-Carlo approach and by Bourlier [23] from an analytical approach and for a 2D problem. By contrast, the multiple reflections between the upper and the lower interfaces of the oil film are taken into account by assuming a locally flat and planar thin oil film. In other words, the two surfaces of the oil film are assumed to be strictly identical and parallel, so that the film can be locally seen as a Fabry–Perot interferometer [see Fig. 6]. This implies that the whole oil film problem can be treated from the single air/oil surface problem, by substituting the Fresnel reflection coefficient of the air/oil single interface for the equivalent Fresnel reflection coefficient of the air/oil/sea film (calculated by considering an infinite number of reflections inside the layer). The calculations are led for IR wavelengths, inside the two window regions 3–5 μm and 8–13 μm: we will consider here the wavelengths 3.4 μm and 10 μm. At these wavelengths, the refractive indices of seawater (taken from the refractive index of pure water by Hale and Querry [24] with the salinity adjustment from Friedman [25]) and oil [26,27] are given in Table 1.

Since, under the GOA, the emissivity depends on the slope probability density function (PDF), the RMS slope along the wind direction of a contaminated sea surface must be calculated. In this paper, a refined and physical model of surface slope damping due to oil films is studied and used: the model of local balance (MLB) [28].

The paper is organized as follows. In Section 2, the equivalent Fresnel reflection coefficient of a locally flat and planar air/oil/sea film is presented, together with its emissivity. In Section 3, the hydrodynamic modeling of the surfaces of clean and contaminated seas is described. In Section 4 the emissivity model is presented, and in Section 5, the emissivity contrast between a clean sea and a contaminated sea is calculated with respect to emission angle, wind speed, wind direction, oil film thickness, oil type, and wavelength. Thus, the detection, characterization, and quantization of the oil are studied. Section 6 gives concluding remarks.

2. Fresnel Reflection Coefficient and Emissivity of Locally Flat and Planar Slab

A. Context

In this section we concentrate on the simple case of the emissivity of flat clean and contaminated seas at

Table 1.

Refractive Indices of Seawater (Taken from Refractive Index of Pure Water by Hale and Querry [24] with Salinity Adjustment from Friedman [25]) and Oil [26,27] for $\lambda = \{3.4; 10\}$ μm, Respectively

Seawater	Heavy Petroleum (No. 20)	Light Petroleum (No. 5)
$1.426 + j0.019$	$1.41 + j0.160$	$1.45 + j0.080$
$1.227 + j0.050$	$1.52 + j0.002$	$1.53 + j0.001$

IR wavelengths, before dealing in the next sections with the case of rough surfaces.

Here, we work at IR wavelengths. More precisely, we are interested in IR window regions. A number of so-called windows exist in the practical range of the IR radiation spectrum. In these windows, transmittance of IR radiation is high. The windows of practical interest for IR optronics systems are 3–5 μm and 8–13 μm; the near-IR window of interest is 0.7–2 μm. Between these windows, there are absorption bands, which are mainly due to the presence of water vapor and carbon dioxide [17]. In this paper, we focus on both IR windows and consider the wavelengths 3.4 μm and 10 μm.

Then, to study the IR emissivity $\epsilon \equiv \epsilon^{\text{flat}}$ of clean and contaminated flat seas at the two wavelengths $\lambda \in \{3.4; 10\}\,\mu$m, we first need to calculate the power Fresnel reflection coefficient $\mathcal{R}$ of clean and contaminated flat seas. Indeed, for flat surfaces emissivity is given by

$$\epsilon^{\text{flat}}(\chi) = 1 - \mathcal{R}(\chi). \tag{1}$$

In what follows, we consider unpolarized emissivity, which implies that the power Fresnel reflection coefficient is unpolarized and defined as

$$\mathcal{R}(\chi) = \frac{|r_V(\chi)|^2 + |r_H(\chi)|^2}{2}, \tag{2}$$

with r_V and r_H being the Fresnel reflection coefficients in vertical (V) and horizontal (H) polarizations, respectively, and χ is the (local) incidence angle onto the (locally) flat clean or contaminated sea; see Fig. 1.

B. Fresnel Reflection Coefficient of Locally Flat and Planar Slab

When an incident plane wave E_i impinges a locally flat and planar thin oil film [see Fig. 1] over the sea surface, it is partially reflected and transmitted at each interface (air/oil and oil/sea). The total reflected field E_r^{tot} back into the incident medium Ω_1 (air of refractive index $n_1 = 1$), is equal to the coherent summation of the successive reflected fields $E_{r,p}$, $E_r^{\text{tot},\infty} = \sum_{p=1}^{\infty} E_{r,p}$.

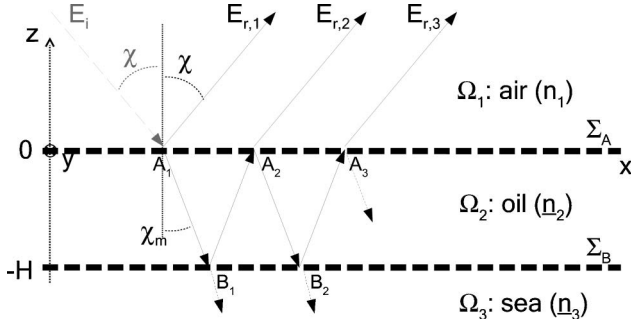

Fig. 1. Illustration of the multiple reflections inside the flat and planar thin film of thickness H with incidence angle χ (local oil film).

1. Calculation of First p Order Reflection Coefficients

Each successive reflected field $E_{r,p}$ depends on the electromagnetic wavelength λ, the complex refractive indices of the oil ($\underline{n_2}$) and of the seawater ($\underline{n_3}$), the local incidence angle χ, the oil film thickness H, and the polarization (vertical, V, or horizontal, H). The corresponding reflection coefficient defined as $r_p = E_p/E_i$ is given by [29,30]

$$\begin{cases} r_1 = r_{12} \\ r_p = t_{12} t_{21} r_{21}^{p-2} r_{23}^{p-1} e^{+j(p-1)\underline{\psi}} \quad \forall p \geq 2 \end{cases}, \tag{3}$$

with

$$\underline{\psi} = 2k_0 \underline{n_2} H \cos \underline{\chi}_m. \tag{4}$$

In Eq. (3), $\{r_{\alpha\beta}, t_{\alpha\beta}\}$ denote the Fresnel reflection coefficient from the medium Ω_α onto the medium Ω_β, and the Fresnel transmission coefficient from the medium Ω_α into the medium Ω_β, respectively. They are defined in V and H polarizations as [29]

$$r_{\alpha\beta}(\chi_\alpha) = \begin{cases} \dfrac{n_\alpha \cos\chi_\beta - n_\beta \cos\chi_\alpha}{n_\alpha \cos\chi_\beta + n_\beta \cos\chi_\alpha} & (V \text{ polarization}) \\ \dfrac{n_\alpha \cos\chi_\alpha - n_\beta \cos\chi_\beta}{n_\alpha \cos\chi_\alpha + n_\beta \cos\chi_\beta} & (H \text{ polarization}) \end{cases}, \tag{5}$$

$$t_{\alpha\beta}(\chi_\alpha) = \begin{cases} [1 - r_{\alpha\beta}(\chi_\alpha)]\dfrac{n_\alpha}{n_\beta} & (V \text{ polarization}) \\ 1 + r_{\alpha\beta}(\chi_\alpha) & (H \text{ polarization}) \end{cases}. \tag{6}$$

$\alpha = \{1,2,3\} \equiv \{\text{air}, \text{oil}, \text{sea}\}$ and $n_\alpha \sin\chi_\alpha = n_\beta \sin\chi_\beta$ (transmission Snell–Descartes law). In Eq. (4), $k_0 = 2\pi/\lambda$ is the electromagnetic wavenumber (inside the vacuum) and $\underline{\chi}_m$ is the complex angle of propagation inside the oil film, obtained from the transmission Snell–Descartes law

$$n_1 \sin\chi = \underline{n_2} \sin\underline{\chi}_m. \tag{7}$$

Indeed, as $\underline{n_2}$ is complex and as the left-hand term of the equation $n_1 \sin\chi$ is real, $\underline{\chi}_m$ must be complex, so that the right-hand term of the equation $\underline{n_2} \sin\underline{\chi}_m$ be real. One can be interested in obtaining the *physical* propagation angle inside the oil film, $\chi_m^{\text{phys}} \in \mathbb{R}$, defined as the direction corresponding to the equiphase surfaces of the wave propagating inside Ω_2. Then it can be shown that this angle χ_m^{phys} is expressed as [31–33]

$$\tan\chi_m^{\text{phys}} = \frac{\sin\chi}{p}, \tag{8}$$

where

$$p = \Re e(\underline{n}_2 \cos \underline{\chi}_m) = \frac{1}{\sqrt{2}}[\sqrt{(\epsilon'_{r2} - \sin^2\chi)^2 + \epsilon''^2_{r2}} + (\epsilon'_{r2} - \sin^2\chi)]^{\frac{1}{2}}, \quad (9)$$

with $\underline{\epsilon}_{r2} = \epsilon'_{r2} + j\epsilon''_{r2}$, in which $\epsilon'_{r2} = \Re e(\underline{\epsilon}_{r2})$ and $\epsilon''_{r2} = \Im m(\underline{\epsilon}_{r2})$. The latter can be expressed with respect to $\underline{n}_2 = n'_2 + jn''_2$ with $n'_2 = \Re e(\underline{n}_2)$ and $n''_2 = \Im m(\underline{n}_2)$ as $\epsilon'_{r2} = \Re e(\underline{n}_2{}^2) = \Re e[(n'_2 + jn''_2)^2] = n'^2_2 - n''^2_2$ and $\epsilon''_{r2} = \Im m(\underline{n}_2{}^2) = \Im m[(n'_2 + jn''_2)^2] = 2n'_2 n''_2$, respectively.

Similarly as for the angle $\underline{\chi}_m$, note that the phase term $\underline{\psi}$ inside Eq. (3) is complex and can be split up into its real, ψ', and imaginary, ψ'', parts, which represent their phase and attenuation components, respectively. By noting the complex term $\underline{n}_2 \cos \underline{\chi}_m = p + jq$, with p and q its real and imaginary parts, respectively, ψ' and ψ'' can be expressed as

$$\psi' = \Re e(\underline{\psi}) = 2k_0 H p, \quad \text{with } p = \Re e(\underline{n}_2 \cos \underline{\chi}_m), \quad (10)$$

$$\psi'' = \Im m(\underline{\psi}) = 2k_0 H q, \quad \text{with } q = \Im m(\underline{n}_2 \cos \underline{\chi}_m). \quad (11)$$

Then, from the imaginary part of the complex phase, ψ'', which gives the attenuation of the wave inside the lossy oil film, the skin depth can be obtained. Usually, the so-called skin depth δ^0_{skin} is defined as

$$\delta^0_{\text{skin}} = 1/(k_0 n'_2). \quad (12)$$

Nevertheless, in our specific case of reflection from the lossy film, first, the classical skin depth must be compared to half the film thickness H because H is traveled twice, and second, we are here in the case of the nonnormal incidence angle χ, so that an appropriate skin depth d_{skin} (which must be compared with H) can be defined as

$$d_{\text{skin}}(\chi) = \frac{1}{2k_0 q}, \quad \text{with } q = \Im m(\underline{n}_2 \cos \underline{\chi}_m), \quad (13)$$

which depends on the local incidence angle χ. Then an attenuation of e^{-1} occurs in the second-order reflection coefficient r_2 for a film thickness equal to our specific skin depth, $H = d_{\text{skin}}$.

2. *Calculation of Global Reflection Coefficient*

The global reflection coefficient at the order P, R_P, resulting from the coherent summation of the first P reflected fields, $E_r^{\text{tot},P} = \sum_{p=1}^{P} E_{r,p}$, is then given by

$$\begin{cases} R_P(\chi) = r_{12} + \sum_{p=2}^{P} (1 - r_{12}^2) r_{21}^{p-2} r_{23}^{p-1} e^{+j(p-1)\psi} \\ R_\infty(\chi) = \dfrac{r_{12} + r_{23} e^{+j\psi}}{1 + r_{12} r_{23} e^{+j\psi}} \end{cases}, \quad (14)$$

by using the relation $t_{12}t_{21} = 1 - r_{12}^2$. The calculation of the global reflection coefficient at the order P requires knowledge of the complex refractive indices of the oil, $\underline{n}_2 = n'_2 + jn''_2$, and of the seawater, $\underline{n}_3 = n'_3 + jn''_3$. They are reported in Table 1 for wavelengths $\lambda = \{3.4, 10\}\,\mu$m. We chose these values of wavelengths in the two IR atmospheric windows $[3; 5]\,\mu$m and $[8; 13]\,\mu$m, for which we have rather precise values of the refractive indices of different kinds of petroleums, namely heavy and light petroleums. It must be noted that the refractive index of the seawater is taken from the refractive index of pure water by Hale and Querry [24] with the salinity adjustment from Friedman [25], by considering a typical ocean with salinity 34.3 ppt and chlorinity 19.0 ppt (ppt refers to parts in 10^{12}). This point was reported in more details by several authors [34–38]. The refractive index of the oil is taken from [26,27].

The real part of n'_3 takes the values 1.426 for $\lambda = 3.4\,\mu$m and 1.227 for $\lambda = 10\,\mu$m, whereas the imaginary part n''_3 takes the values 0.019 for $\lambda = 3.4\,\mu$m and 0.050 for $\lambda = 10\,\mu$m. Thus, in thermal IR window regions, the imaginary part of the refractive index of the seawater is small as compared to unity and to its real part. In the IR band, the refractive index of oil has been studied by several authors, and especially Al'perovich *et al.* [26], in the region $\lambda \in [0.25; 25]\,\mu$m. They studied the refractive index of various petroleum samples and highlighted that they are characterized by different values of n'_2 and n''_2. Here we will consider two petroleums that are typical of two distinct groups: petroleum no. 2, which is a typical heavy petroleum, and petroleum no. 5, which is a typical light petroleum. For both cases, like that for the seawater, the imaginary part of the refractive index of the oil is rather small as compared to unity and to its real part: it is rather small at $\lambda = 3.4\,\mu$m and very small at $\lambda = 10\,\mu$m. Thus, the physical propagation angle χ_m^{phys} inside Ω_2, given by Eq. (8), can be approximated by $\sin\chi_m^{\text{phys}} \simeq \sin\chi/n'_2$. Then it can be calculated that the use of this approximation leads to a maximum relative error on the value of χ_m^{phys} of 0.79% and 0.17% for heavy and light petroleums at $\lambda = 3.4\,\mu$m, respectively, and of 8.0×10^{-5}% and 1.9×10^{-5}% for heavy and light petroleums at $\lambda = 10\,\mu$m, respectively.

In Fig. 2, the unpolarized power reflection coefficient $\mathcal{R}_P$ is plotted in dB scale [$10\log_{10}(\ldots)$] versus the local incidence angle χ for $P = \{1, 2, \infty\}$. It is defined as

$$\mathcal{R}_P(\chi) = \frac{|R_{P,V}(\chi)|^2 + |R_{P,H}(\chi)|^2}{2}. \quad (15)$$

The unpolarized power reflection coefficient at the oil/sea interface $|r_{23}|^2$ and the unpolarized power reflection coefficient of a clean sea surface $|r_{13}|^2$ are also plotted for comparison. $\lambda = 10\,\mu$m, $H = 50\,\mu$m, and a heavy petroleum is considered. It can be seen that only the first two orders contribute to the total reflected unpolarized power since $\mathcal{R}_2 \approx \mathcal{R}_\infty$. This is

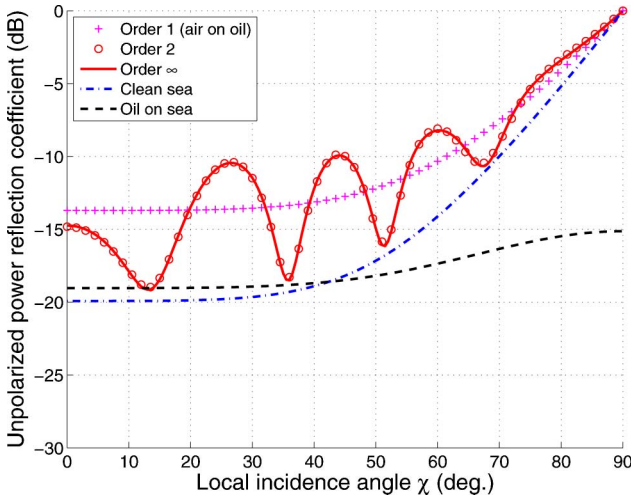

Fig. 2. (Color online) Unpolarized power reflection coefficient (dB) versus the local incidence angle χ (°) for $\lambda = 10\,\mu$m, $H = 50\,\mu$m, and for a heavy petroleum.

due to the fact that the unpolarized power reflection coefficient of the oil/sea interface $|r_{23}|^2 \ll 1$ [indeed, it is always inferior to 0.031 here in the case of Fig. 2]. Thus, the equivalent reflection coefficient R_∞ given by Eq. (14) can be approximated by the first two orders R_2:

$$R_\infty \approx R_2 = r_{12} + (1 - r_{12}^2) r_{23} e^{+j\psi}. \tag{16}$$

In this case, it can be noted that the so-called skin depth, defined as $\delta_{\text{skin}}^0 = 1/(k_0 n_2')$, is equal to 796 μm, which is significantly greater than $H = 50\,\mu$m. Then it could be concluded that attenuation is negligible. Nevertheless, in our specific case of reflection from the lossy film, we have to consider the appropriate skin depth d_{skin} defined in Eq. (13), which depends on the local incidence angle χ. Then, in the case represented in Fig. 2 where $\lambda = 10\,\mu$m, d_{skin} ranges from 300 μm to 398 μm. As a consequence, from Fig. 2 where $H = 50\,\mu$m, the attenuation term $e^{-\psi''}$, with $\psi'' = H/d_{\text{skin}}$, ranges from 0.846 to 0.882, which is weak attenuation but not negligible.

Figure 2 also highlights a general significant difference between a clean sea and a contaminated sea. Then, when computing the emissivity given for flat surfaces by Eq. (1), this makes the oil film rather easy to detect at this wavelength. For the parameters given in Table 1, other simulations with different thicknesses and for light petroleum (not reported in this paper) show similar results for the same wavelength $\lambda = 10\,\mu$m. The main appearing differences are the frequency of the oscillations of the unpolarized power reflection coefficient with respect to χ: for increasing film thickness H or for increasing real part of the oil refractive index, n_2', the frequency of the oscillations increases. Moreover, for increasing H, the amplitude of the oscillations slightly decreases, owing to the attenuation term $e^{-\psi''}$, with $\psi'' = H/d_{\text{skin}}$. Then, for $H = 100\,\mu$m, $e^{-\psi''}$ ranges from 0.716 to 0.778 (to be compared with a range from 0.846 to 0.882 with $H = 50\,\mu$m).

In Fig. 3, the unpolarized power reflection coefficient $\mathcal{R}_P$ is plotted in dB scale [$10\log_{10}(\ldots)$] versus the local incidence angle χ for the same parameters as in Fig. 2, except for the wavelength $\lambda = 3.4\,\mu$m. Compared to Fig. 2 where the first two orders contributed to the total power reflection coefficient $\mathcal{R}_\infty$, here it can be seen that only the first order contributes to $\mathcal{R}_\infty$: $\mathcal{R}_1 \approx \mathcal{R}_\infty$. Even if the unpolarized power reflection coefficient of the oil/sea interface $|r_{23}|^2$ is decreased [indeed, it is always inferior to 0.025 here in the case of Fig. 2], this is not the main reason and not sufficient for neglecting the orders higher than the first one. The difference is mainly due to the attenuation term $e^{-\psi''}$, with $\psi'' = H/d_{\text{skin}}$. More precisely, it is rather the modification of the imaginary part of the refractive index, n_2'', which is increased for heavy petroleum by a factor of 80, which mainly explains the fact that all orders higher than the first one can be neglected. Indeed, here for $\lambda = 3.4\,\mu$m, d_{skin} ranges from 1.2 μm to 1.7 μm, so that the attenuation term $e^{-\psi''}$ ranges from 1.02×10^{-18} to 1.44×10^{-13}. Figure 3 also highlights a general low difference between a clean sea and a contaminated sea for all local incidence angles χ, and especially for high χ. Then, when computing the emissivity given for flat surfaces by Eq. (1), this makes the oil film hard to detect at this wavelength. For the parameters given in Table 1, other simulations with different thicknesses and for light petroleum (not reported in this paper) show similar results for the same wavelength $\lambda = 3.4\,\mu$m. Here, even for much thinner oil films, such as $H = 10\,\mu$m, the attenuation term remains very weak (it ranges in this case from 0.252×10^{-3} to 2.70×10^{-3}), so that the orders higher than the first one remain negligible, and the oscillations observed at $\lambda = 10\,\mu$m are damped (and eliminated) here at $\lambda = 3.4\,\mu$m.

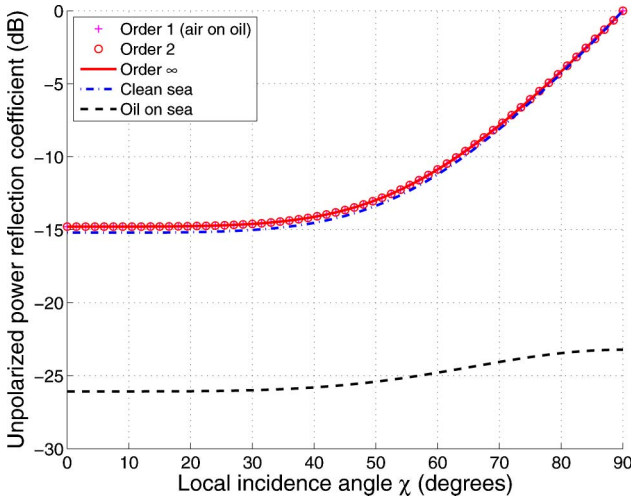

Fig. 3. (Color online) Same parameters as in Fig. 2, except for $\lambda = 3.4\,\mu$m.

3. Hydrodynamic Modeling of Surfaces of Clean and Contaminated Seas

In this section, the hydrodynamic modeling of clean and contaminated seas is led, by considering that the two (air/oil and oil/sea) interfaces of the contaminated case obey the same statistics, i.e., have the same surface height PDF and spectrum [in fact, they can even be considered identical and parallel, as illustrated in Fig. 6]. For both clean and contaminated seas, the surface height PDF is assumed to be Gaussian. For a clean sea, the surface spectrum is assumed to obey the Elfouhaily *et al.* spectrum model [39].

In what follows, the surface spectrum of a contaminated sea is studied more thoroughly. Two hydrodynamic models of surface wave damping due to oil films are presented to calculate the slope variances of a contaminated sea surface. The first one, namely the Lombardini *et al.* model [40–42], is a rather simple model that is independent of the oil film thickness H. The second one, namely the MLB [28], is a more refined and physical model, which takes the impact of oil films on the wind waves into account.

A. Thickness-Independent Model: Lombardini *et al.* Model [40–42]

In [40–42], Lombardini *et al.* demonstrated that ripples on a water surface covered by an oil film exhibit a damping effect in the surface wave spectrum, which is characterized by a maximum located in the gravity-capillary region, around the surface wave frequency (pulsation) of $\omega = 20\pi\,\mathrm{rad/s}$.

This damping effect is expressed by an attenuation coefficient y_{Lomb} [42], which is usually called the Marangoni viscous damping coefficient [43,44] and is expressed by [42]

$$y_{\mathrm{Lomb}}(k; E_0, \omega_D) = \frac{1 \pm 2\tau + 2\tau^2 - X + Y(X+\tau)}{1 \pm 2\tau + 2\tau^2 - 2X + 2X^2}, \tag{17}$$

where

$$\tau = \left(\frac{\omega_D}{2\omega}\right)^{1/2} \quad X = \frac{E_0 k^2}{\rho(2\nu\omega^3)^{1/2}} \quad Y = \frac{E_0 k}{4\nu\rho\omega}, \tag{18}$$

are dimensionless quantities, and

$$\omega = (\zeta k^3/\rho + gk)^{1/2}, \tag{19}$$

is the dispersion law. E_0 denotes the elasticity modulus (N/m), $\rho = 10^3\,\mathrm{kg/m^3}$ the water density, $\nu = 10^{-6}\,\mathrm{m^2/s^2}$ the kinematic viscosity, $\zeta = 74\times 10^{-3}\,\mathrm{N/m}$ the surface tension, $g = 9.81\,\mathrm{m/s^2}$ the acceleration of gravity, and k the surface wavenumber. Furthermore, ω_D is a characteristic pulsation, which, for soluble films, depends on the diffusional relaxation, and for insoluble films, depends on the structural relaxation between intermolecular forces.

In Eq. (17), inside $\pm$, $+$ refers to soluble films, whereas $-$ refers to insoluble films. In conclusion, under this model, y_{Lomb} depends on the surface frequency (pulsation) ω or the surface wavenumber k (related to each other by the dispersion law) and on the oil parameters $\{\omega_D, E_0\}$.

According to Lombardini *et al.* [42], the contaminated sea surface height spectrum S_{cont} is related to the clean sea surface height spectrum S_{clean} by the ratio

$$S_{\mathrm{cont,Lomb}}(k; u_{10}, \phi, E_0, \omega_D) = \frac{S_{\mathrm{clean}}(k; u_{10}, \phi)}{y_{\mathrm{Lomb,s}}(k; E_0, \omega_D)}. \tag{20}$$

The term $y_{\mathrm{Lomb,s}}$ is taken here to deal with more general cases when the sea surface is only partially covered in oil. Thus, $y_{\mathrm{Lomb,s}}$ is related to y_{Lomb} by the relation

$$y_{\mathrm{Lomb,s}} = (1 - F + F/y_{\mathrm{Lomb}})^{-1}, \tag{21}$$

with F being the fractional filling factor, i.e., the ratio of the area covered by film with respect to the considered total area. In what follows, when dealing with the contaminated case, we will consider a total coverage, i.e., $F = 1$. Here, for the clean sea height spectrum, the sea is assumed to be fully developed and the Elfouhaily *et al.* [39] model is used, which is defined as

$$S_{\mathrm{clean}}(k; u_{10,}\phi) = M(k)[1 + \Delta(k)\cos(2\phi)]/(2\pi), \tag{22}$$

where $M(k)$ and $\Delta(k)$ are the isotropic and anisotropic parts of the spectrum. They depend on the wind speed defined at 10 m above the sea u_{10}. ϕ stands for the wind direction. From Eq. (17), it must be noted that y_{Lomb} is assumed to be independent of the wind direction ϕ.

Here, a sea covered by an insoluble oil film is considered (for soluble films, see [45], for instance). Then ω_D depends on the structural relaxation between intermolecular forces. It must be noted that contrary to simulations led in [42], which consider organic films, we have here the case of oil films. This implies that the simulation parameters of the oil (ω_D and E_0) to be used can take *a priori* different values than the typical ones in [42]. This was confirmed recently from experiments [46,47] in which it was concluded that the elasticity values E_0 are smaller for oil films than for organic films and smaller than 10 mN/m [46,47]. Moreover, physically, the characteristic pulsation ω_D should be small for insoluble homogeneous oil films.

Thus, in what follows, two different cases of the Lombardini *et al.* damping model [42] will be presented for the contaminated case, and compared to a more refined and physical model, namely, the MLB [28], which is described in the following.

Table 2. Values of Physical Parameters PP Obtained from Laboratory and Field Experiments with Oil, Used in Numerical Simulations Presented Here

Oil Volume Viscosity ν_{oil}	Surface Tension σ_+	Interface Tension σ_-	Surface Elasticity E_+	Interface Elasticity E_-	Surface Viscosity μ_+	Interface Viscosity μ_-
0.1–0.5 cm^2/s	30 mN/m	20 mN/m	0	5 mN/m	0	0

B. Thickness-Dependent Physical Model: Model of Local Balance [28]

The Lombardini *et al.* damping model [40–42], which was used in previous work for radar applications [18,45], considers that the sea surface is only partially covered by thin films and, most important, that wind speed is extremely small $u_{10} < 1$ m/s [28]. However, real marine slicks may be large, and when an impact of oil films on the surface waves is analyzed, one should take into account wind input, energy output due to viscosity, wave breaking, nonlinear wave-wave interaction, and so on. However, in the cm – mm wave range characteristic, times of nonlinear wave-wave interactions are much larger than the wind growth rate and the damping coefficient due to viscosity; see [28]. Thus, in the first assumption, wave-wave interaction can be neglected, and the wind wave spectrum is assumed to be determined by local balance of wave energy inputs and outputs in k space. Such a model is analyzed in [28], and the spectrum contrast (the ratio between spectra on the clean and contaminated surfaces) is defined by the following expression:

$$y_{\mathrm{MLB}} = \frac{S_{\mathrm{clean}}(k;u_{10},\phi)}{S_{\mathrm{cont}}(k;u_{10},\phi,H,PP)} = \left[\frac{\beta(u^*,k)-\gamma_{\mathrm{clean}}(k)}{\beta(u^*,k)-\gamma_{\mathrm{cont}}(k,H,PP)}\right]^n, \quad (23)$$

$$\text{with} \begin{cases} n=+1 & \text{if } \beta>\gamma, \\ n=-1 & \text{if } \beta<\gamma, \end{cases}$$

where $\beta(u^*,k)$ is the wind growth rate [48] with u^* the friction velocity, which depends on the wind velocity u_{10}, $\gamma_{\mathrm{clean}}(k) = 2\nu k^2$ is the wave viscous damping on the clean surface (with ν the kinematic viscosity of water), and $\gamma_{\mathrm{cont}}(k,H,PP)$ is the wave viscous damping on the contaminated surface, covered by an oil film of thickness H and with physical parameters denoted as PP. For monomolecular films ($H = 0$), wave viscous damping depends only on the rheological parameters E_0 and ω_D of the oil film. In this case, the wave viscous damping is connected with the viscous damping coefficient given in the Lombardini *et al.* damping model (17) as

$$\gamma_{\mathrm{cont}} = 2\nu k^2 \times y_{\mathrm{Lomb}}(k,E_0,\omega_D). \quad (24)$$

In the general case ($H \neq 0$), the wave viscous damping γ_{cont} depends on the film thickness H and on physical parameters PP: oil volume viscosity ν_{oil}, surface (air/oil) and interface (oil/water) tensions σ_+ and σ_-, respectively, surface and interface elasticities E_+ and E_-, respectively, and viscosities μ_+ and μ_-, respectively [47,49]. In this case, the wave viscous damping can be described in the frame of a two-layer liquid model; see Appendix A. The values of the physical parameters PP obtained from laboratory and field experiments with oil are located in Table 2; see [46,47].

The system of linear Navier–Stokes equations with corrresponding boundary conditions and physical parameters from Table 2 for a two-layer liquid [46,47] was numerically calculated for different upper layer thicknesses H (for more details, see Appendix A). The obtained wave viscous damping $\gamma_{\mathrm{cont}}(k,H,PP)$ was used to calculate the spectrum contrast (23). Numerous field experiments demonstrated that the spectrum contrast does not depend on the angle between the wind direction and the observation direction ϕ [28]. So in Eq. (23) we use wind growth rate inwind direction. We used the same expression for clean sea height spectrum as in Section 3.A, Eq. (22) to calculate the spectrum on the contaminated surface:

$$S_{\mathrm{cont,MLB}}(k;u_{10},\phi,H,PP) = \frac{S_{\mathrm{clean}}(k;u_{10},\phi)}{y_{\mathrm{MLB}}}. \quad (25)$$

Thus, the difference between the Lombardini *et al.* model and the MLB is that the contaminated spectrum $S_{\mathrm{cont}} = S_{\mathrm{cont,Lomb}}$ [with $y = y_{\mathrm{Lomb}}$ calculated from Eq. (17)] depends on E_0 and ω_D for the Lombardini *et al.* model, whereas $S_{\mathrm{cont}} = S_{\mathrm{cont,MLB}}$ [with $y = y_{\mathrm{MLB}}$ calculated from Eq. (23)] depends on H and PP for the MLB.

First, the slope spectrum k^2S of the surfaces of clean and contaminated seas is plotted for two different cases of the Lombardini *et al.* damping model [42] and compared with the MLB [28] with two different film thicknesses. Then the RMS slopes of the surfaces of clean and contaminated seas are plotted for wind speeds u_{10} ranging from 2 to 10 m/s.

C. Slope Spectrum and Slope Variances

In Fig. 4, the *slope* spectrum isotropic part of a clean and a contaminated sea surface, $k^2S_{\mathrm{clean}} = k^2M(k)$ and $k^2S_{\mathrm{cont}} = k^2M(k)/y$, respectively, is plotted versus the surface wavenumber k. For a contaminated sea surface, $y = y_{\mathrm{Lomb}}$ corresponds to the Lombardini *et al.* damping model, whereas $y = y_{\mathrm{MLB}}$ corresponds to the MLB. The two different cases of the Lombardini *et al.* damping model are taken as $\{\omega_D = 0\,\mathrm{rad/s}, E_0 = 1\,\mathrm{mN/m}\}$ and $\{\omega_D = 1\,\mathrm{rad/s}, E_0 = 2\,\mathrm{mN/m}\}$ for an insoluble film with $F = 1$. They are compared with the MLB for a heavy oil with viscosity 0.5 cm^2/s, having a film thickness of either

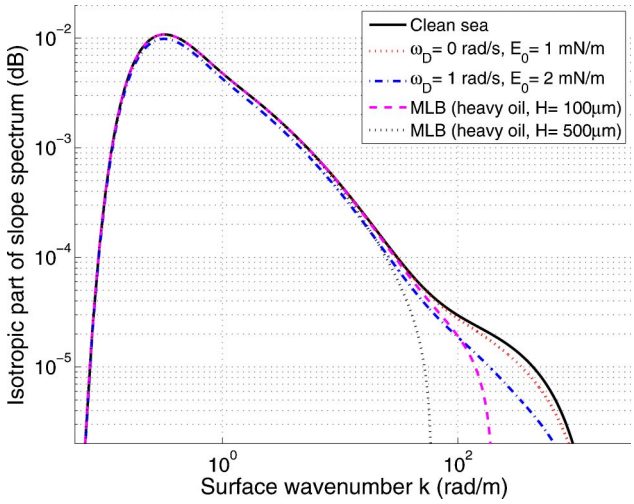

Fig. 4. (Color online) Isotropic part of the slope spectrum of clean and contaminated sea surfaces versus the surface wavenumber k. For the contaminated sea, two cases of the Lombardini *et al.* damping model are compared with two cases of the MLB, with a heavy oil of viscosity $0.5\,\mathrm{cm}^2/\mathrm{s}$ having a film thickness of $H = 100\,\mu\mathrm{m}$ or $H = 500\,\mu\mathrm{m}$. The wind speed is $u_{10} = 6\,\mathrm{m/s}$.

$H = 100\,\mu\mathrm{m}$ or $H = 500\,\mu\mathrm{m}$. These values of the Lombardini *et al.* model are taken so that the damping ratio has a similar behavior as the one obtained from measurements [46,47] and most importantly, to match with the result of the MLB [28]. The wind speed is $u_{10} = 6\,\mathrm{m/s}$. As expected, it can be seen that the oil film significantly damps the high frequencies, which corresponds to the capillary waves.

Compared to higher values of E_0, which typically correspond to organic films, the damping in high frequencies is, in general, weaker for oil films than for organic films. Moreover, the damping is stronger for $\{\omega_D = 1\,\mathrm{rad/s}, E_0 = 2\mathrm{mN/m}\}$ than for $\{\omega_D = 0\mathrm{rad/s}, E_0 = 1\,\mathrm{mN/m}\}$. More precisely, an increase of ω_D mainly implies a decrease of the slope spectrum around its maximum, and an increase of E_0 mainly implies a decrease of the high frequencies of the spectrum. Then, compared to the MLB results, it can be concluded that to best match the MLB, the Lombardini *et al.* damping model must have $\omega_D < 1\,\mathrm{rad/s}$ and be close to 0, as expected. Nevertheless, the best value of E_0 would be hard to determine, as the Lombardini *et al.* damping model cannot properly approximate the MLB values for high frequencies, highlighting the limitations of this model to deal with oil films for this typical film thickness.

The simulation results of the MLB for two different thicknesses $H = 100\,\mu\mathrm{m}$ and $H = 500\,\mu\mathrm{m}$ show that an increase of the film thickness H implies, in general, a stronger damping of the surface spectrum. More precisely, the limit surface wavenumber k from which a (strong) damping of the surface spectrum is observed decreases. This phenomenon is also true for an increase of the oil viscosity, corresponding to heavier fuel oils. In what follows, the impact of the oil damping on the surface RMS slopes is studied.

From Eq. (22), Bourlier and Berginc [50] showed that the slope variance σ_{sX}^2 along the angle ϕ between wind direction and observation azimuthal direction (which is usually called wind direction for the sake of simplicity), is given by

$$\sigma_{sX}^2 = \alpha + \beta\cos(2\phi), \tag{26}$$

where

$$\alpha = \frac{1}{2}\int_0^{+\infty}\frac{M(k)}{y}k^2\mathrm{d}k, \qquad \beta = \frac{1}{4}\int_0^{+\infty}\frac{M(k)\Delta(k)}{y}k^2\mathrm{d}k, \tag{27}$$

with $y = y_{\mathrm{Lomb}}$ for the Lombardini *et al.* damping model and $y = y_{\mathrm{MLB}}$ for the MLB. In Fig. 5, the RMS slopes defined in the upwind direction $\phi = 0$, σ_{sx}, and crosswind direction $\phi = \pi/2$, σ_{sy}, defined as

$$\sigma_{sx} = \sqrt{\alpha+\beta}, \qquad \sigma_{sy} = \sqrt{\alpha-\beta}, \tag{28}$$

of the surfaces of clean and contaminated seas are plotted versus the wind speed u_{10}, in the range 2–10m/s. The oil film is characterized by the same parameters as in Fig. 4. In addition, the results are compared with the Cox and Munk [16] experimental model, given for a contaminated sea by

$$\begin{cases} \sigma_{sx}^2 = 0.005 + 0.78\times10^{-3}u_{12} \pm 0.002 \\ \sigma_{sy}^2 = 0.003 + 0.84\times10^{-3}u_{12} \pm 0.002 \end{cases}, \tag{29}$$

where u_{12} is the wind speed at 12.5 meters above the sea (the vertical lines represent the error bars of the Cox and Munk experimental model). In [16], the oil film is a mixture consisting of 40% used crankcase oil, 40% diesel oil, and 20% fish oil (with mean oil film thickness of the order of $20\,\mu\mathrm{m}$ [18]). It is then

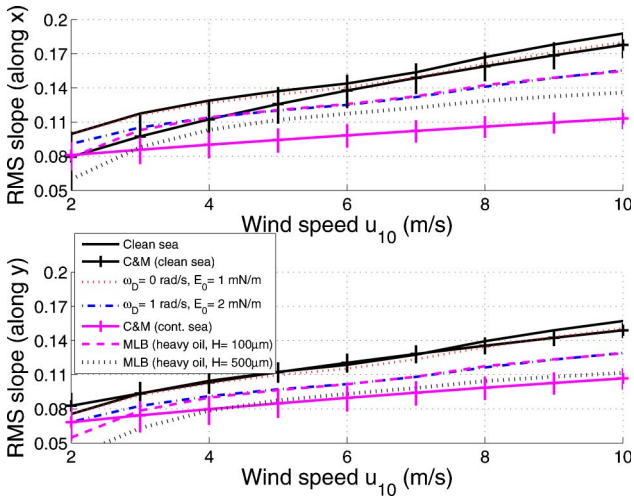

Fig. 5. (Color online) RMS slopes in the x and y directions, σ_{sx} and σ_{sy}, of clean and contaminated sea surfaces [with the same parameters as in Fig. 4] versus the wind speed u_{10} in the range 2–10 m/s: comparison with the Cox and Munk experimental model.

difficult to relate the parameters $\{\omega_D, E_0\}$ of the Lombardini *et al.* model in Eq. (17) to this mixture. The same remark holds for the MLB. It can be seen that the RMS slope of the contaminated (air/oil and oil/sea) interfaces is lower than that of the clean air/sea interface. Nevertheless, the differences are not very significant: in particular, compared to the Cox and Munk experimental model [16], the results of the two cases of Lombardini *et al.* model are significantly higher, especially for the higher wind speeds u_{10} and for the RMS slope along the upwind direction (at the top). The same remark holds for the MLB with thickness $H = 100\,\mu$m, which gives results very close to the second case of the Lombardini *et al.* model. A physical explanation of this difference can be given. Indeed, the Cox and Munk experimental results [16] were led for a film which cannot strictly be considered as oil, as described previously. As a consequence, the comparison with the Cox and Munk experimental results is mainly qualitative. The results for the MLB with a larger thickness $H = 500\,\mu$m highlight a good agreement with the Cox and Munk experimental results, and in particular for the y direction (crosswind). Here, the comparison is also mainly qualitative, as we compare the films with different chemical compositions and with *a priori* not equal physical behaviors (especially viscosity). Nevertheless, this confirms the coherence of the model. Moreover, comparing the two MLB results for $H = 100\,\mu$m and $H = 500\,\mu$m, it confirms the observation done in Fig. 4: a stronger damping at high surface wavenumber for $H = 500\,\mu$m implies a stronger damping of surface slopes, leading to a decrease of the RMS slopes.

In what follows, for the contaminated sea, the surface spectrum obtained from the MLB will be considered.

In the next section, the influence of rough oil films on rough sea surfaces in the unpolarized emissivity is calculated and compared with the emissivity of rough clean sea surfaces.

4. Unpolarized Infrared Emissivity of Clean and Contaminated Seas

Previously we focused on a flat and planar film. In this section, let us consider the real case of rough interfaces. The two interfaces of the contaminated sea are strictly identical and parallel between each other as depicted in Fig. 6, which is realistic for thin oil films over sea surfaces (this approach is widely used for microwave applications [18,51–53]). Following the results of Section 2 for locally flat surfaces and by using the results of Section 3 to take the surface roughness into account (with the MLB for the contaminated sea), the behavior of the emissivity of contaminated rough seas by comparison with clean rough seas can be predicted.

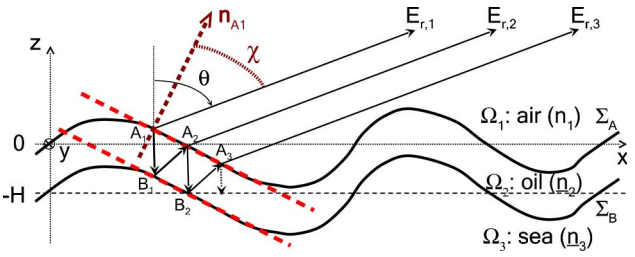

Fig. 6. (Color online) Emissivity with multiple reflection from the contaminated sea: representation of the first three scattered fields $E_{r,1}$, $E_{r,2}$, and $E_{r,3}$

A. Description of Method

Since the electromagnetic wavelength λ is much smaller than the surface mean curvature radius R_c, the tangent plane approximation (usually called the Kirchhoff approximation) can be applied. As a consequence, each interface can be locally replaced by its infinite tangent plane, at each point of the rough surface. Thus, the emissivity can be obtained from the local emissivity for flat interfaces, $\epsilon^{\text{flat}}(\chi) = 1 - \mathcal{R}(\chi)$ (1), with χ being the local incidence angle.

Moreover, with the electromagnetic wavelength λ being also much smaller than the surface RMS height σ_h, the GOA can be applied. For a single interface, Bourlier [17] calculated the unpolarized emissivity of an anisotropic rough sea by taking the shadowing effect into account and by neglecting the multiple reflections that can be involved at the rough surface. The emissivity depends then on the unpolarized power reflection coefficient $\mathcal{R}(\chi)$ and on the slope PDF $p_s(\gamma_x, \gamma_y)$ (with γ_x and γ_y being the local slopes in the upwind and crosswind directions, respectively), which requires knowledge of the RMS surface slopes σ_{sx} and σ_{sy} in the upwind and crosswind directions, respectively. Here, Gaussian slope PDF is assumed, with RMS slopes calculated from Eqs. (26)–(28), and by considering the MLB for the contaminated sea.

B. Unpolarized Emissivity

The unpolarized emissivity with shadowing effect of a single interface is then given by [17]

$$\epsilon(\theta,\phi) = \frac{1}{1+\Lambda(\theta,\phi)} \int_{-\infty}^{+\mu} \mathrm{d}\gamma_X \int_{-\infty}^{+\infty} [1 - \mathcal{R}(\chi)] p_s(\gamma_x,\gamma_y) \left(1 - \frac{\gamma_X}{\mu}\right) \mathrm{d}\gamma_Y, \tag{30}$$

with $\chi \equiv \chi(\theta,\phi,\gamma_x,\gamma_y)$ being the local incidence angle (i.e., the angle between the local normal to the surface and the direction of observation), given by the relation

$$\cos\chi(\theta,\phi,\gamma_x,\gamma_y) = \frac{\left(1-\frac{\gamma_X}{\mu}\right)\cos\theta}{(1+\gamma_X^2+\gamma_Y^2)^{\frac{1}{2}}}. \tag{31}$$

$\{\theta \in [0;\pi/2], \phi \in [0;2\pi]\}$ stand for the elevation and azimuthal emission angles, respectively, and $\mu = \cot\theta$ is the observation direction slope. The wind direction is taken as $\phi_{\text{wind}} = 0$. For Gaussian statistics, the slope PDF p_s is given by

$$p_s(\gamma_x,\gamma_x)=\frac{1}{2\pi\sigma_{sx}\sigma_{sy}}\exp\left(-\frac{\gamma_x^2}{2\sigma_{sx}^2}-\frac{\gamma_y^2}{2\sigma_{sy}^2}\right). \quad (32)$$

$\{\gamma_x,\gamma_y\}$ are the surface slopes in the upwind and crosswind directions, respectively, and $\{\sigma_{sx}^2,\sigma_{sy}^2\}$ are their associated slope variances. $\{\gamma_X,\gamma_Y\}$ are the surface slopes along the ϕ direction and the orthogonal direction, respectively, obtained from $\{\gamma_x,\gamma_y\}$ by a rotation of an angle ϕ such that

$$\begin{cases}\gamma_X=+\gamma_x\cos\phi+\gamma_y\sin\phi\\ \gamma_Y=-\gamma_x\sin\phi+\gamma_y\cos\phi\end{cases}. \quad (33)$$

$1/(1+\Lambda)$ corresponds to the *propagation* shadowing effect, and the restriction over the integration over the variable γ_X, $\gamma_X<+\mu$, corresponds to the *angular* shadowing effect. For Gaussian statistics, Λ is expressed as [17]

$$\Lambda(v)=\frac{\exp(-v^2)-v\sqrt{\pi}\mathrm{erfc}(v)}{2v\sqrt{\pi}},$$
$$\text{with } v=\frac{|\cot\theta|}{\sqrt{2}[(\sigma_{sx}\cos\phi)^2+(\sigma_{sy}\sin\phi)^2]^{1/2}}. \quad (34)$$

In Eq. (30), $\mathcal{R}$ is the unpolarized power reflection coefficient given by Eq. (2). For a clean sea, $\{R_{P,V},R_{P,H}\}$ are substituted for $\{r_{13,V},r_{13,H}\}$ (air/sea interface).

Thus, for a contaminated sea, the unpolarized emissivity is also obtained from Eq. (30) with the same shadowing, but the unpolarized power reflection coefficient is given by Eq. (15). Then $\{R_{P,V},R_{P,H}\}$ are substituted for $\{R_{\infty,V},R_{\infty,H}\}$, where R_∞ is expressed by Eq. (16). Moreover, the RMS slopes in the PDF slope calculation take different values, as described previously and illustrated in Fig. 5.

In the numerical results to follow in next section, the oil film is described by the MLB [28].

5. Numerical Results

A. Comparison Between Rough and Flat Seas

First, let us study the influence of the roughness of the surfaces in the unpolarized emissivities of clean and contaminated seas, ϵ_{clean} and ϵ_{cont}, respectively. In Fig. 7, ϵ_{clean} and ϵ_{cont} are plotted with respect to the emission angle θ, for $\lambda=10\,\mu$m, $u_{10}=6\,$m/s, and $\phi=0$. A comparison is also made with the case of flat surfaces, corresponding to $u_{10}=0\,$m/s. The contaminated sea is a heavy oil film of thickness $H=50\,\mu$m and viscosity $0.5\,\text{cm}^2/\text{s}$, described for nonzero wind speed by the MLB. In Fig. 7(b), the emissivity relative contrast of the flat case with respect to the rough case is represented. Also, the horizontal dotted curve plotted for an emissivity relative contrast of 0.5% corresponds to the limit of detectability of a sensor with 0.3 K accuracy.

For a clean sea, as shown by Bourlier *et al.* (see Fig. 7 of [17] for more details), for emission angles

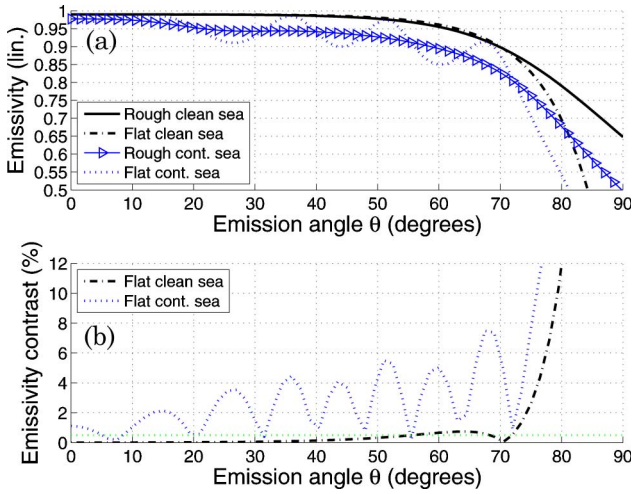

Fig. 7. (Color online) (a) Unpolarized emissivity of clean and contaminated seas and (b) emissivity contrast between clean and contaminated seas versus the emission angle θ for $\lambda=10\,\mu$m, $u_{10}=6\,$m/s, $\phi=0$. The contaminated sea is a heavy oil film of thickness $H=50\,\mu$m, described by the MLB. A comparison is also made with the case of flat interfaces, corresponding to $u_{10}=0\,$m/s.

smaller than at least 50°, the difference between the flat and the rough cases is small enough to be neglected. Then, for these emission angles, the emissivity can be evaluated from the simple flat case. As the emission angle increases, the emissivity relative contrast significantly increases from 70°, owing to the surface roughness. By contrast, for a contaminated sea, the difference between the flat and rough cases is rather significant and cannot be neglected, in general, for this typical configuration. Indeed, oscillations of the emissivity can be observed with respect to θ for the flat case, contrary to the rough case where the oscillations are strongly smoothed and are nearly invisible. Thus, the emissivity relative contrast is rather significant in general, and the rough case cannot be evaluated from the simple flat case. The same general observations and conclusions between rough and flat cases can be held for other film thicknesses. Moreover, as studied more thoroughly in the following, there is a general significant difference between clean and contaminated seas, making the oil slick detectable.

Figure 8 presents simulation results for the same parameters as in Fig. 7, except for the wavelength $\lambda=3.4\,\mu$m. For a clean sea, the same general observations and conclusions can be led. Here, for a contaminated sea, contrary to $\lambda=10\,\mu$m, there is no oscillation of the emissivity of the flat curve, making the difference between the flat and rough cases significant only for similar emission angles θ to that of the clean sea. Thus, here, for both cases the difference between flat and rough curves is significant only for $\theta>70°$, and increases rapidly as θ increases. The same general observations and conclusions between rough and flat cases can be held for other film thicknesses, as the results are the same even for flat surfaces of the oil film. Moreover, as can be seen, there is

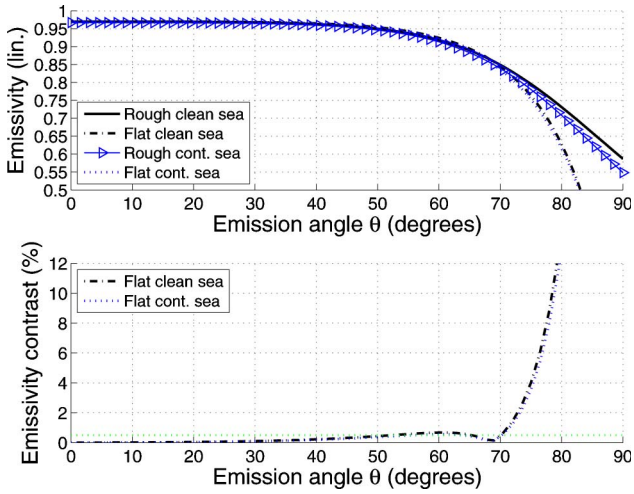

Fig. 8. (Color online) Same parameters as in Fig. 7, except for the wavelength is $\lambda = 3.4\,\mu$m.

a significant difference between clean and contaminated seas only for high emission angles, $\theta \gtrsim 75°$.

The next subsection studies the influence of wind speed and of the oil film thickness, especially for $\lambda = 10\,\mu$m (indeed, the oil film thickness does not have a strong influence at $\lambda = 3.4\,\mu$m), the other parameters (mainly wind direction and oil type) being kept constant. Moreover, in all the following, the influence of varying the physical parameters on the emissivities is studied separately, which in practice would correspond to knowing the other parameters.

B. Influence of Wind Speed and of Oil Film Thickness

In Fig. 9, the same variations as in Fig. 7 are plotted, but for a lower wind speed, $u_{10} = 4\,$m/s. Moreover, the flat cases are not represented any more, but different oil film thicknesses are represented, $H = \{0, 10, 50, 100, 500\}\,\mu$m. Then the emissivity relative contrast is plotted here in Fig. 9(b) for the contaminated case with reference to the clean case. The horizontal dotted curve corresponding to the limit of detectability of a sensor with 0.3 K accuracy remains.

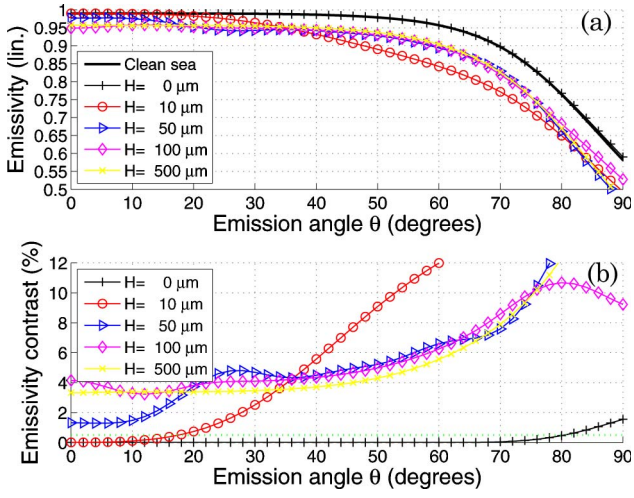

Fig. 9. (Color online) (a) Unpolarized emissivity of clean and contaminated seas and (b) emissivity contrast between clean and contaminated seas versus the emission angle θ for $\lambda = 10\,\mu$m, $u_{10} = 4\,$m/s, and $\phi = 0$. The contaminated sea is a heavy oil film of thicknesses $H = \{0, 10, 50, 100, 500\}\,\mu$m, described by the MLB.

First, compared to Fig. 7, let us compare the two curves with right-pointing triangles, which both correspond to the contaminated case with film thickness $H = 50\,\mu$m. For the lower wind speed $u_{10} = 4\,$m/s in Fig. 9, the oscillations of the emissivity are less smoothed than for $u_{10} = 6\,$m/s in Fig. 7. This confirms the fact that the oscillations of the emissivity that may occur for the contaminated sea with flat surfaces are increasingly smoothed as the wind speed increases, because the surface roughness increases. Second, by comparing the results for various oil thicknesses with the clean sea case, the differences are, in general, significant, making the oil film detectable. The case $H = 0$ is an oil film with zero thickness, which would physically correspond to a clean sea whose surface is the same as the ones of the contaminated sea. Indeed, as explained earlier, the oil film makes the capillary waves of the surface damped compared to the clean surface. Then the case $H = 0$ highlights the influence of the capillary wave damping on the emissivity. Thus, the emissivity relative contrast in Fig. 9(b) highlights that this surface wave damping has a significant influence on the emissivity only for very high emission angles, $\theta \gtrsim 80°$. Third, by comparing the different oil film thicknesses between one another, they have general different behaviors with respect to the emission angle θ. For the other parameters kept constant (in particular, wind speed and direction and oil type), which is equivalent, in practice, to assume them as known, this makes the distinction between the thicknesses possible and the oil thickness estimation conceivable, especially if measurements are made at several emission angles θ. The distinction is, in general, easier for the lower thicknesses and for low wind speeds, because of the oscillations with respect to θ.

In Fig. 10, the same variations as in Fig. 9 are plotted, but for a higher wind speed, $u_{10} = 8\,$m/s. Here, compared to the clean sea surface, the damping of the capillary waves of the contaminated sea surfaces is more significant compared to Fig. 9 because of the higher wind speed. Indeed, as the wind speed increases from 4 m/s to 8 m/s, the difference in the surface RMS surface slopes between clean and contaminated seas increases; see Fig. 5. This implies that the case $H = 0$ highlights a significantly higher difference with the clean sea here for $u_{10} = 8\,$m/s than for $u_{10} = 4\,$m/s. Similarly to what is seen in in Fig. 9, by comparing the results for various oil thicknesses with the clean sea case, the differences are, in general, significant, making the oil film detectable. Moreover, as expected, the oscillations that appeared in Fig. 9(b) are smoothed here as u_{10} is increased. Thus, the distinction between the different thicknesses is a bit more difficult for rather thick films, like here between $H = 50\,\mu$m, $H = 100\,\mu$m, and $H = 500\,\mu$m for $15° \lesssim \theta \lesssim 75°$.

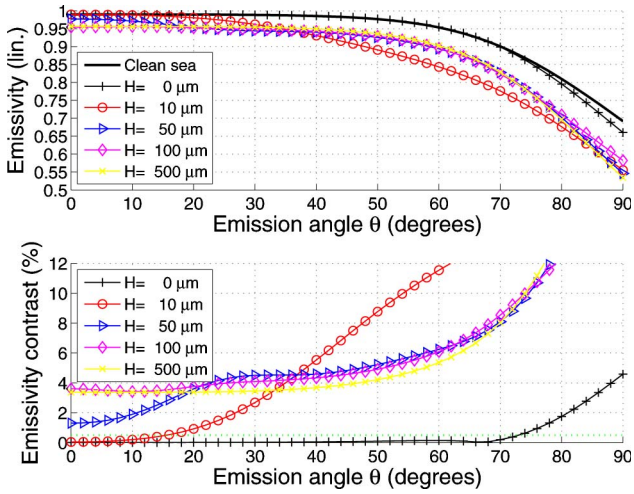

Fig. 10. (Color online) Same parameters as in Fig. 9, except for the wind speed is $u_{10} = 8\,\mathrm{m/s}$.

For the other wavelength $\lambda = 3.4\,\mu\mathrm{m}$, as explained in the previous subsection for flat surfaces, the emissivity of a flat contaminated sea does not vary with the oil film thickness, making the oil thickness estimation impossible at this wavelength for a zero wind condition, $u_{10} = 0$. Moreover, the difference between clean and contaminated seas is significant only for high emission angles θ, for which the oil film can be detected. Nevertheless, for rough surfaces, as illustrated in Fig. 11, for the same parameters as in Fig. 10 except for the wavelength $\lambda = 3.4\,\mu\mathrm{m}$, the oil thickness estimation is possible for high emission angles θ, here for $\theta \gtrsim 75°$. This is due to the fact that the hydrodynamic damping modeled by the MLB, which depends on the oil film thickness H, influences the emissivity for high θ. This thickness estimation is easier for increasing wind speed, because of stronger hydrodynamic damping. Moreover, one interesting feature is that for high θ, the emissivity relative contrast is directly and only related to the hydrodynamic damping (through the RMS slopes), making the

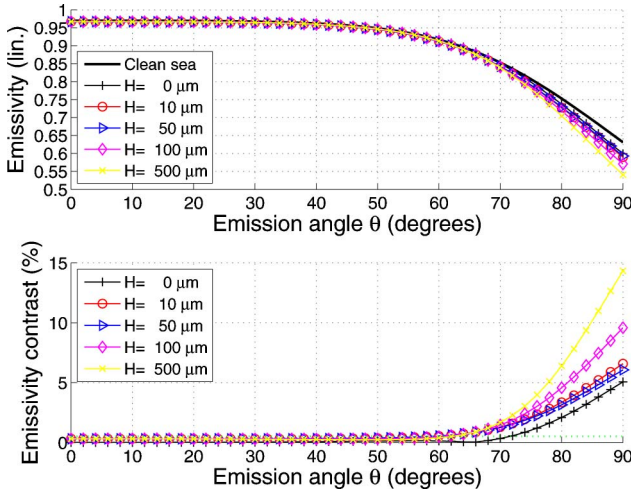

Fig. 11. (Color online) Same parameters as in Fig. 10, except for the wavelength is $\lambda = 3.4\,\mu\mathrm{m}$.

thickness estimation not too difficult for moderate wind speeds as illustrated here.

In conclusion, the oil film detection and quantization (i.e., thickness estimation) is, in general, much easier at $\lambda = 10\,\mu\mathrm{m}$ than at $\lambda = 3.4\,\mu\mathrm{m}$. The next subsection studies the possibility of making the distinction between different types of oils (here, between heavy and light oils).

C. Oil Slick Type Characterization

In Fig. 12, the same variations as in Fig. 7 are plotted, but for both wavelengths $\lambda = \{3.4; 10\}\,\mu\mathrm{m}$. Moreover, both heavy (with viscosity $0.5\,\mathrm{cm^2/s}$) and light (with viscosity $0.1\,\mathrm{cm^2/s}$) fuel oils are plotted, in order to study the possibility of oil slick type characterization. The clean sea cases are not reported here for the sake of clarity [but implicitly appear in Fig. 12(b)]. For the lower wavelength $\lambda = 3.4\,\mu\mathrm{m}$, the emissivity relative contrast with the clean sea is, in general, rather low and could be not sufficient for oil detection with average-quality sensors. Indeed, it is close to the limit of detectability given for sensors with 0.3 K accuracy, that is to say 0.5%, except from relatively low-grazing emission angles $\theta \gtrsim 60°$, where the relative contrast increases and becomes significant. Moreover, light and heavy fuel oils are not distinguishable, unless for very good quality sensors at very low grazing angles $\theta \gtrsim 80°$–$85°$, where small differences appear. By contrast, for the higher wavelength $\lambda = 10\,\mu\mathrm{m}$, oil detection is always possible because the emissivity relative contrast is always greater than 2%. Moreover, light and heavy fuel oils can be distinguished at least for low or high emission angles, in particular for $\theta \lesssim 15°$ or for $\theta \gtrsim 75°$.

Thus, it is, in general, much better to work at $\lambda = 10\,\mu\mathrm{m}$ rather than at $\lambda = 3.4\,\mu\mathrm{m}$ for both oil slick detection and characterization. Indeed, the

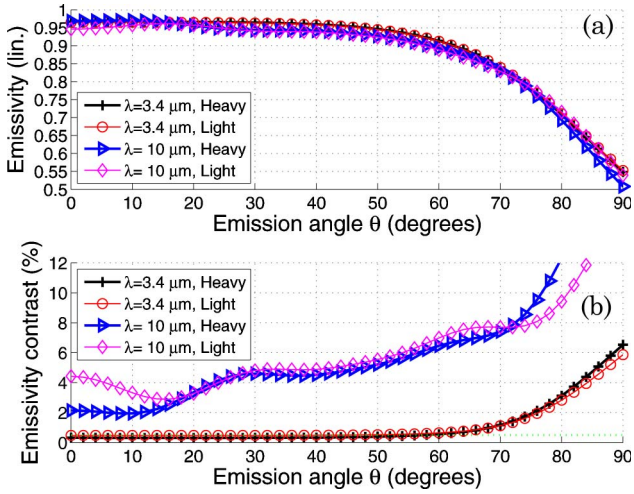

Fig. 12. (Color online) (a) Unpolarized emissivity of contaminated seas and (b) emissivity contrast between clean and contaminated seas versus the emission angle θ for $u_{10} = 6\,\mathrm{m/s}$, $\phi = 0$, and $\lambda = \{3.4, 10\}\,\mu\mathrm{m}$, and for both light and heavy fuel oils. The contaminated sea is of thickness $H = 50\,\mu\mathrm{m}$, described by the MLB.

characterization is hard at $\lambda = 3.4\,\mu$m and possible only for very high θ, where the hydrodynamic damping, which is different for the two oil types, has a direct influence on emissivity (through the RMS slopes).

Eventually, the last subsection studies the influence of the observation azimuthal direction with respect to the wind direction, given by ϕ, on the emissivity of clean and contaminated seas.

D. Influence of Observation Direction

In Fig. 13, the unpolarized emissivity of clean and contaminated seas with respect to the observation direction versus wind direction angle ϕ is plotted for $\theta = 80°$, $u_{10} = \{4, 8\}$ m/s, and $\lambda = 10\,\mu$m. The contaminated sea is a heavy fuel oil (with viscosity $0.5\,\text{cm}^2/\text{s}$) of thickness $H = 50\,\mu$m, described by the MLB.

For a clean sea [17] as well as for a contaminated sea, Fig. 13 shows that the emissivity is symmetric with respect to the downwind direction, i.e., $\epsilon(\theta, \pi - \phi) = \epsilon(\theta, \pi + \phi)$. This symmetry can be explained as follows: the emissivity computed from Eq. (30) depends on the slope γ_Y, because the angle χ and the slope PDF $p_s(\gamma_x, \gamma_y) \equiv p_s(\gamma_X, \gamma_Y)$ depend on γ_Y. Inasmuch as the slope γ_Y is much smaller than unity, χ can be approximated in $\cos\chi$ as $\cos\chi \approx (1 - \gamma_X/\mu) \times \cos\theta/(1 + \gamma_X)^{1/2}$, which is independent of γ_Y. Thus, the slope PDF $p_s(\gamma_X, \gamma_Y)$ can be integrated over γ_Y to obtain the marginal PDF $p_s(\gamma_X)$, expressed from Eq. (9) of [17]. The resulting expression of the emissivity is then {see Eq. (27) of [17] for a clean sea}

$$\epsilon(\theta, \phi) \approx \frac{1}{1 + \Lambda(\theta, \phi)} \times \int_{-\infty}^{+\mu} [1 - \mathcal{R}(\chi)] p_s(\gamma_X) \left(1 - \frac{\gamma_X}{\mu}\right) \mathrm{d}\gamma_X. \quad (35)$$

In addition, as the slope PDF $p_s(\gamma_X)$ is symmetric with respect to the downwind direction, the emissivity has the same property. The computation of the emissivity then requires only one numerical integration.

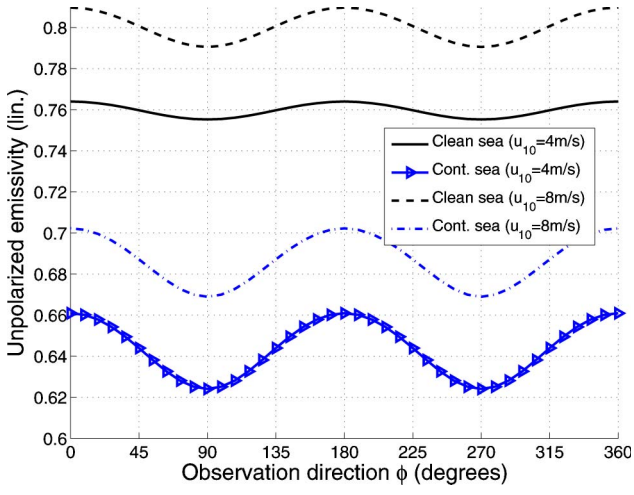

Fig. 13. (Color online) Unpolarized emissivity of clean and contaminated seas versus the observation direction ϕ for $\theta = 80°$, $u_{10} = \{4, 8\}$ m/s, and $\lambda = 10\,\mu$m. The contaminated sea is a heavy fuel oil of thickness $H = 50\,\mu$m, described by the MLB.

For $\phi \in [0; 360]°$, Fig. 13 shows that the emissivity varies as a cosine function with a nonzero mean value [i.e., $\epsilon(\theta, \phi) \approx \epsilon_0(\theta) + \epsilon_2(\theta)\cos(2\phi)$], where its minimum occurs in the crosswind directions $\phi = 90°$ and $\phi = 270°$, for which the RMS slope $\sigma_{sX} = \sigma_{sy}$ is minimum. Conversely, its maximum occurs in the upwind ($\phi = 0°$) and downwind ($\phi = 180°$) directions, for which $\sigma_{sX} = \sigma_{sx}$ is maximum. In addition, it can be seen that $\epsilon(\theta, 0) = \epsilon(\theta, \pi)$ and $\epsilon(\theta, \pi/2) = \epsilon(\theta, 3\pi/2)$ because, for a Gaussian process, the slope PDF is even. If higher-order statistics is taken into account like in [17] for a clean sea, the emissivity is more sensitive to the wind direction for high wind speeds. The emissivity can be modeled with respect to the observation direction versus wind direction angle ϕ (usually called wind direction for simplicity) as

$$\epsilon(\theta, \phi) \approx \epsilon_0(\theta) + \epsilon_1(\theta)\cos(\phi) + \epsilon_2(\theta)\cos(2\phi), \quad (36)$$

where $\{\epsilon_{0,1,2}(\theta)\}$ can be found from the values of $\epsilon(\theta, 0)$, $\epsilon(\theta, \pi/2)$, and $\epsilon(\theta, \pi)$ as

$$\epsilon_0(\theta) = [\epsilon(\theta, 0) + \epsilon(\theta, \pi) + 2\epsilon(\theta, \pi/2)]/4, \quad (37)$$

$$\epsilon_1(\theta) = [\epsilon(\theta, 0) - \epsilon(\theta, \pi)]/2, \quad (38)$$

$$\epsilon_2(\theta) = [\epsilon(\theta, 0) + \epsilon(\theta, \pi) - 2\epsilon(\theta, \pi/2)]/4. \quad (39)$$

$\epsilon_0(\theta)$ corresponds to the emissivity of an isotropic surface, $\epsilon_1(\theta)$ corresponds to the asymmetry between the upwind and the downwind directions [for the Gaussian statistics considered here, it vanishes because $\epsilon(\theta, 0) = \epsilon(\theta, \pi)$], and $\epsilon_2(\theta)$ corresponds to the asymmetry between the upwind and the crosswind directions.

In fact, the anisotropic effect becomes appreciable for large emission angles. For Gaussian statistics, Bourlier *et al.* [17] showed that emissivity can be fitted as $\epsilon(\theta, \phi) = \epsilon_0(\theta) + \epsilon_2(\theta)\cos(2\phi)$, in which $\epsilon_2(\theta)$ is an increasing function of θ. The same general observations and conclusions can be held for $\lambda = 3.4\,\mu$m.

6. Conclusion

This paper presented the unpolarized emissivity of thin oil films over anisotropic Gaussian seas based on the following assumptions:

- The GOA is assumed to be valid.
- The non-Gaussianity of the surfaces is neglected.
- The multiple reflections at each interface (air/oil and oil/sea) are neglected.
- The multiple reflections inside the oil film are taken into account.

- The thin oil film is assumed to be made up of two strictly identical and parallel interfaces, which form a local so-called Fabry–Perot interferometer.

Since the refractive index contrast between the oil and the sea is small (and especially for $\lambda = 3.4\,\mu$m, see Table 1), the incident intensity is mostly transmitted into the sea, which implies that only the first-order, $E_{r,1}$, and the second-order, $E_{r,2}$, reflected fields [see Fig. 1] contribute to the total reflected field. For $\lambda = 3.4\,\mu$m, only $E_{r,1}$ contributes to the total reflected field, owing to the losses inside the oil film.

Since, under the GOA, the emissivity depends on the slope PDF, the slope variance along the wind direction of the surfaces of a contaminated sea must be calculated. In this paper, one hydrodynamic model of surface damping due to the oil film is then studied, namely the Lombardini *et al.* model [40–42] and compared with a more refined and physical model, namely the MLB [28]. The parameters of the Lombardini *et al.* model are chosen to be consistent with the results of the MLB but highlight the limitations of this simple model for oil films.

Then numerical simulations are shown to investigate the influence of the physical parameters (mainly wind speed, oil film thickness, oil type, as well as wind direction) on the emissivities of both clean and contaminated seas. The influence of each parameter is studied separately by keeping the other parameters constant, which, in practice, would correspond to knowing them. The results show that the emissivity contrast between a clean sea and a contaminated sea is significant for $\lambda = 10\,\mu$m and increases when the emission angle increases. It is significant for $\lambda = 3.4\,\mu$m only for high emission angles. Also, for $\lambda = 10\,\mu$m, the contrast varies with respect to the oil film thickness mainly because of the interferences between the two first-order reflected fields $E_{r,1}$ and $E_{r,2}$, allowing oil film thickness estimation. As the wind speed increases, the surfaces become rougher and the interferences are smoothed, implying increasingly difficult thickness estimation. Nevertheless, at very high emission angles θ and for both wavelengths, the hydrodynamic damping, which depends on the film thickness, has a strong influence on the emissivity through the RMS slopes, and in particular for the higher wind speeds. Thus, it is rather easy to estimate the film thickness, in particular for $\lambda = 3.4\,\mu$m, for which damping is the only parameter that influences the emissivity.

Besides, the numerical results show that the emissivity varies nearly insignificantly with the nature of the oil film (heavy or light) at $\lambda = 3.4\,\mu$m (except for very high θ, because of the hydrodynamic damping), contrary to $\lambda = 10\,\mu$m where significant differences appear, in particular for low or high emission angles θ. Thus, oil type characterization is possible mostly at this latter wavelength. Last, it was observed that the emissivity has a cosine function behavior with respect to the wind direction.

The method used to obtain the present model can be applied for the calculation of the reflectivity. Indeed, like the emissivity, the reflectivity of a single rough interface depends on the power of Fresnel reflection coefficients. Thus, using the same assumptions as for the derivation of the emissivity, the reflectivity of thin films can be obtained from substituting the Fresnel reflection coefficients of a single interface for the ones of a thin film.

Calculation of Wave Viscous Damping γ_{cont} in Model of Local Balance

The wave viscous damping was calculated in the frame of the model of two Newtonian viscous fluid layers. The motion was assumed in two dimensions (x, z), nonlinear effects were neglected (see [49]), and the linearized continuity and momentum equations in upper and lower layers are

$$U_x + W_z = 0, \tag{A1}$$

$$U_t + P_x = \nu \nabla^2 U, \tag{A2}$$

$$W_t + P_z = \nu \nabla^2 W, \tag{A3}$$

with U and W being the horizontal and vertical velocity components, respectively, P is the pressure, and ν is the volume viscosity. The subscript $(\cdot)_+$ refers to either the upper fluid layer (film) or to the free surface (air/oil), where appropriate, and the subscript $(\cdot)_-$ refers, correspondingly, to either the lower fluid or to the interface (oil/sea). Other subscripts indicate partial differentiation with respect to the spatial coordinates x and z and to time t. We use the boundary conditions for undisturbed levels.

Conditions at the free surface $z = H$, with H being the upper layer (film) thickness are

$$W_+ = Z_{+t}, \tag{A4}$$

$$\rho_+ \nu_+ (U_{+z} + W_{+x}) = E_+ \xi_{xx} + \mu_+ \xi_{xxt}, \tag{A5}$$

$$P_+ - gZ - 2\nu_+ W_{+z} + (\sigma_+/\rho_+) Z_{xx} = 0, \tag{A6}$$

$$U_+ = \xi_t, \tag{A7}$$

with Z being the free surface level, ρ is the density (in either fluid), E_+ and μ_+ are the surface elasticity and viscosity, respectively, ξ is the horizontal fluid particle displacement, and σ_+ is the surface tension.

Conditions at the interface $z = 0$ are

$$W_+ = W_- = H_t, \tag{A8}$$

$$U_+ = U_-, \tag{A9}$$

$$\rho_+\nu_+(U_{+z}+W_{+x})+E_-\xi_{xx}+\mu_-\xi_{xxt}=\rho_-\nu_-(U_{-z}+W_{-z}), \tag{A10}$$

$$\rho_+(P_+-gZ-2\nu_+W_{+z})=\rho_-(P_--gH-2\nu_-W_{-z})+\sigma_-H_{xx}, \tag{A11}$$

with E_- and μ_- being the interface elasticity and viscosity, respectively, and σ_- is the interface tension.

Velocities, pressure, and horizontal and vertical displacements $U, W, P, Z, H, \ldots$ are assumed to be proportional to $\exp(-ikx+nt)$, where k is the wavenumber, $n=i\omega-\gamma$ with ω are the wave frequency (pulsation) and γ is the wave viscous damping; the depth of the lower fluid is assumed to be infinite. If all parameters PP (oil volume viscosity ν_{oil}, surface and interface tensions σ_+ and σ_-, respectively, surface and interface elasticities E_+ and E_-, respectively, and viscosities μ_+ and μ_-, respectively), the thickness of the upper layer H, and the wavenumber k are initially determined, we have two unknown parameters, ω and γ, which can be obtained as a decision of the system.

When $H=0$ (monomolecular film), this system has a simple well-known decision [42,54,55]. When the thickness of the upper layer is less than the thickness of the viscous sublayer ($H \ll \sqrt{\nu/\omega}$), the expression of the wave viscous damping is adduced in [49].

Here, since the wind wave spectrum stretch from meter to millimeters, it is not always correct to use the approximation $H \ll \sqrt{\nu/\omega}$, so we numerically calculated this system and obtained the dependences of wave viscous damping on wavenumber for different film thicknesses H.

The work has been supported by the Russian Foundation for Basic Research (RFBR) (project 10-05-00101). The authors would like to thank the reviewers for their useful comments, which helped improve the quality of the manuscript.

References

1. V. Wismann, M. Gade, W. Alpers, and H. Hühnerfuss, "Radar signature of marine mineral oil spills measured by an airborne multi-radar," Int. J. Remote Sensing **19**, 3607–3623 (1998).
2. H. A. Espedal and O. M. Johannessen, "Detection of oil spills near offshore installations using synthetic aperture radar (SAR)," Int. J. Remote Sensing **21**, 2141–2144 (2000).
3. X. Wu and W. Smith, "Emissivity of rough sea surface for 8–13 μm: modeling and verification," Appl. Opt. **36**, 2609–2619 (1997).
4. C. R. Zeisse, C. P. McGrath, K. M. Littfin, and H. G. Hughes, "Infrared radiance of the wind-ruffled sea," J. Opt. Soc. Am. A **16**, 1439–1452 (1999).
5. D. E. Freund, R. I. Joseph, D. J. Donohue, and K. T. Constantikes, "Numerical computations of rough sea surface emissivity using the interaction probability density," J. Opt. Soc. Am. A **14**, 1836–1849 (1997).
6. C. Bourlier, G. Berginc, and J. Saillard, "Theoretical study on two-dimensional Gaussian rough sea surface emission and reflection in the infrared frequencies with shadowing effect," IEEE Trans. Geosci. Remote Sensing **39**, 379–392 (2001).
7. Z. Otremba, "Selected results of light field modeling above the sea surface covered by thin oil film," in *Computer Simulation and Boundary Field Problems, Environmental Simulations* (Riga Technical University, 1999), Vol. 41.
8. Z. Otremba and J. Piskozub, "Modelling of the optical contrast of an oil film on a sea surface," Opt. Express **9**, 411–416 (2001).
9. Z. Otremba and J. Piskozub, "Modeling the remotely sensed optical contrast caused by oil suspended in the sea water column," Opt. Express **11**, 2–6 (2003).
10. Z. Otremba and J. Piskozub, "Modelling the bidirectional reflectance distribution function (BRDF) of seawater polluted by an oil film," Opt. Express **12**, 1671–1676 (2004).
11. V. Byfield, "Optical remote sensing of oil in the marine environment," Ph.D. thesis (School of Ocean and Earth Science, University of Southampton, 1998).
12. G. Kara, "Remote sensing of oil films on the sea surface," Turkish J. Mar. Sci. **8**, 27–40 (2002).
13. W.-C. Shih and A. B. Andrews, "Modeling of thickness dependent infrared radiance contrast of native and crude oil covered water surfaces," Opt. Express **16**, 10535–10542 (2008).
14. W.-C. Shih and A. B. Andrews, "Infrared contrast of crude-oil-covered water surfaces," Opt. Lett. **33**, 3019–3021 (2008).
15. N. de Beaucoudrey, P. Schott, and C. Bourlier, "Detection of oil slicks on sea surface depending on layer thickness and sensor frequency," in *Proceedings of the 2003 IEEE International Geoscience and Remote Sensing Symposium* (IEEE, 2003), pp. 2741–2743.
16. C. Cox and W. Munk, "Measurement of the roughness of the sea surface from photographs of the sun's glitter," J. Opt. Soc. Am. **44**, 838–850 (1954).
17. C. Bourlier, "Unpolarized infrared emissivity with shadow from anisotropic rough sea surfaces with non-Gaussian statistics," Appl. Opt. **44**, 4335–4349 (2005).
18. N. Pinel, N. Déchamps, and C. Bourlier, "Modeling of the bistatic electromagnetic scattering from sea surfaces covered in oil for microwave applications," IEEE Trans. Geosci. Remote Sensing **46**, 385–392 (2008).
19. K. Lamkaouchi, "Water: a dielectric standard. permittivity of water-petrol mixtures at microwave frequencies," Ph.D. thesis (Bordeaux I University, 1992) (in French).
20. C. Cox and W. Munk, "Statistics of the sea surface derived from sun glitter," J. Mar. Res. **13**, 198–227 (1954).
21. C. Cox and W. Munk, "Slopes of the sea surface deduced from photographs of sun glitter," Bulletin of the Scripps Institution of Oceanograpy of the University of California **6**, 401–488 (1956).
22. B. Henderson, J. Theiler, and P. Villeneuve, "The polarized emissivity of a wind-roughened sea surface: a Monte Carlo model," Remote Sens. Environ. **88**, 453–467 (2003).
23. C. Bourlier, "Unpolarized emissivity with shadow and multiple reflections from random rough surfaces with the geometric optics approximation: application to Gaussian sea surfaces in the infrared band," Appl. Opt. **45**, 6241–6254 (2006).
24. G. Hale and M. Querry, "Optical constants of water in the 200 nm to 200 μm wavelength region," Appl. Opt. **12**, 555–563 (1973).
25. D. Friedman, "Infrared characteristics of ocean water (1.5–15 μ)," Appl. Opt. **8**, 2073–2078 (1969).
26. L. Al'perovich, A. Komarova, B. Narziev, and V. Pushkarev, "Optical constants of petroleum samples in the 0.25–25 μ range," J. Appl. Spectrosc. **28**, 491–494 (1978).

27. V. Osadchy, K. Shifrin, and I. Gurevich, "The airborne identification of oil films at the Caspian sea surface using CO_2 lidar," Oceanol. Acta **22**, 51–56 (1999).
28. S. Ermakov, S. Salashin, and A. Panchenko, "Film slicks on the sea surface and some mechanisms of their formation," Dyn. Atmos. Oceans **16**, 279–304 (1992).
29. M. Born and E. Wolf, *Principles of Optics*, 6th ed. (Pergamon, 1980).
30. N. Pinel, C. Bourlier, and J. Saillard, "Forward radar propagation over oil slicks on sea surfaces using the Ament model with shadowing effect," Prog. Electromagn. Res. **PIER-76**, 95–126 (2007).
31. P.-F. Combes, *Micro-Ondes—Cours et Exercices avec Solutions. Tome 1: Lignes, Guides et Cavités* (Dunod, 1996).
32. R. D. Roo and C.-T. Tai, "Plane wave reflection and refraction involving a finitely conducting medium," IEEE Antennas Propag. Mag. **45**, 54–61 (2003).
33. N. Pinel, N. Déchamps, C. Bourlier, and J. Saillard, "Bistatic scattering from one-dimensional random rough homogeneous layers in the high-frequency limit with shadowing effect," Waves Random Complex Media **17**, 283–303 (2007).
34. J. Wu, "Effects of atmospheric stability on ocean ripples: A comparison between optical and microwave measurements," J. Geophys. Res. **96**, 7265–7269 (1991).
35. W. Smith, R. Knuteson, H. Revercomb, W. Feltz, H. Howell, W. Menzel, N. Nalli, O. Brown, J. Brown, P. Minnett, and W. McKeown, "Observations of the infrared radiative properties of the ocean implications for the measurement of sea surface temperature via satellite remote sensing," Bull. Am. Meteorol. Soc. **77**, 41–51 (1996).
36. K. Masuda, "Infrared sea surface emissivity including multiple reflection effect for isotropic Gaussian slope distribution model," Remote Sens. Environ. **103**, 488–496 (2006).
37. L. Pontier and C. Dechambenoy, "Détermination des constantes optiques de l'eau liquide entre 1 et 40 μm. application au calcul de son pouvoir réflecteur et de son émissivité," Ann. Geophys. **22**, 633–641 (1966).
38. D. Wieliczka, S. Weng, and M. Querry, "Wedge shaped cell for highly absorbent liquids: infrared optical constants of water," Appl. Opt. **28**, 1714–1719 (1989).
39. T. Elfouhaily, B. Chapron, K. Katsaros, and D. Vandemark, "A unified directional spectrum for long and short wind-driven waves," J. Geophys. Res. **102**, 15781–15796 (1997).
40. R. Cini and P. Lombardini, "Damping effect of monolayers on surface wave motion in a liquid," J. Colloid Interface Sci. **65**, 387–389 (1978).
41. R. Cini, P. Lombardini, C. Manfredi, and E. Cini, "Ripples damping due to monomolecular films," J. Colloid Interface Sci. **119**, 74–80 (1987).
42. P. Lombardini, B. Fiscella, P. Trivero, C. Cappa, and W. Garrett, "Modulation of the spectra of short gravity waves by sea surface films: slick detection and characterization with a microwave probe," J. Atmos. Ocean. Technol. **6**, 882–890 (1989).
43. W. Alpers and H. Huhnerfuss, "The damping of ocean waves by surface films: a new look at an old problem," J. Geophys. Res. **94**, 6251–6265 (1989).
44. M. Gade, W. Alpers, H. Huhnerfuss, V. Wismann, and A. Lange, "On the reduction of the radar backscatter by oceanic surface films: scatterometer measurements and their theoretical interpretation," Remote Sens. Environ. **66**, 52–70 (1998).
45. M. Ayari, A. Coatanhay, and A. Khenchaf, "The influence of ripple damping on electromagnetic bistatic scattering by sea surface," in *Proceedings of the 2005 International Geoscience and Remote Sensing Symposium* (IEEE, 2005), pp. 1345–1348.
46. S. Ermakov, "Possibilities of identification of oil films using radar probing of the sea surface," in *Proceedings of the 2008 IEEE/OES US/EU-Baltic International Symposium (BALTIC)* (IEEE, 2008), pp. 1–6.
47. I. Sergievskaya and S. Ermakov, "On wave damping due to oil films," in *Proceedings of the 2008 IEEE/OES US/EU-Baltic International Symposium (BALTIC)* (IEEE, 2008), pp. 1–6.
48. W. Plant, "A relationship between wind stress and wave slope," J. Geophys. Res. **87**, 1961–1967 (1982).
49. A. Jenkins and S. Jacobs, "Wave damping by a thin layer of viscous fluid," Phys. Fluids **9**, 1256–1264 (1997).
50. C. Bourlier and G. Berginc, "Microwave analytical backscattering models from randomly anisotropic sea surface—comparison with experimental data in C and Ku bands," in *Progress in Electromagnetics Research*, D. J. A. Kong, ed. (EMW Publishing, 2002), Vol. 37, pp. 31–78.
51. G. Franceschetti, A. Iodice, D. Riccio, G. Ruello, and R. Siviero, "SAR raw signal simulation of oil slicks in ocean environments," IEEE Trans. Geosci. Remote Sensing **40**, 1935–1949 (2002).
52. M. Migliaccio, M. Tranfaglia, and S. Ermakov, "A physical approach for the observation of oil spills in SAR images," IEEE J. Oceanic Eng. **30**, 496–507 (2005).
53. I. Fuks and V. Zavorotny, "Polarization dependence of radar contrast for sea surface oil slicks," IEEE Radar Conf. 503–508 (2007).
54. V. G. Levich, "The theory of waves by surface-active materials," (in Russian) Zh. Eksp. Teor. Fiz., 10, 1296–1304 (1940). English translation, Acta Physicochimica URSS, 14, 307–328 (1941).
55. V. G. Levich, *Physicochemical Hydrodynamics* (Prentice Hall, 1962).